2019

A Design of a Material Assembly in Space-Time Generating and Storing Energy

Mihhail Berezovski
Embry-Riddle Aeronautical University, berezovm@erau.edu

Stan Elektrov
Worcester Polytechnic Institute

Konstantin Lurie
Worcester Polytechnic Institute

A Design of a Material Assembly in Space-Time Generating and Storing Energy

Mihhail Berezovski*, Stan Elektrov, Konstantin Lurie†

Professor Jüri Engelbrecht is widely known as an outstanding scholar in various branches of mechanics and mathematical physics. Through many years, he has been one of the main contributors to the intensive development of science and academic education in his homeland Estonia and far beyond it, on the European scale. His public service is commensurate with his scientific merits. Jüri's sphere of interests is vast, and it always belonged to the cutting edge of mechanics and thermodynamics. This is the reason why we decided to submit our work to Jüri's jubilee collection of papers; we dedicate it to our dear colleague and friend with the hope that it may get along with his long-time professional aspirations.

1 Abstract

The paper introduces a theoretical background of the mechanism of electromagnetic energy and power accumulation and its focusing in narrow pulses travelling along a transmission line with material parameters variable in 1D-space and time. This mechanism may be implemented due to a special material geometry- a distribution of two different dielectrics in a spatio-temporal checkerboard. We concentrate on the practically reasonable means to bring this mechanism into action in a device that may work both as energy generator and energy storage. The basic ideas discussed below appear to be fairly general; we have chosen their electromagnetic implementation as an excellent framework for the entire concept.

2 Introduction

This paper is about a physical implementation of a novel concept in material science and technology termed *dynamic materials* (DM) [1],[2]. DM are not the materials in a traditional sense: they are defined as material substances with properties that may change in *space and time*. Particularly, we may speak about formations assembled from traditional material constituents with space-time variable properties. This understanding is unusual because DM should be thought of as substances that are not fabricated once for all, but rather brought into the scene and maintained by being properly operated in space and time. Specifically, the temporal property change is possible only due to an exchange of mass, momentum, and energy between the DM and the environment. To put it in brief, *a DM is a thermodynamically open system; only its union with the environment may be considered as closed.* The very notion of DM makes sense only when it is perceived as a spatial-temporal entity, and this is the main difference between DM and ordinary materials that exist as dead substances, i.e., their properties do not change in time. Contrary to DM, the ordinary materials appear to be thermodynamically closed.

Living tissue represents a natural example of DM; as to a man made implementation, this has become possible due to recent progress in technology that allows for the *property tuning*, specifically on a micro- and nano-scale. Some technical means towards such tuning are detailed in [3],[4],[5],[6],[7],[8]; at this point we only mention that

*Department of Mathematics, Embry-Riddle Aeronautical University, Daytona Beach, FL, mihhail.berezovski@erau.edu
†Department of Mathematics, Worcester Polytechnic Institute, Worcester, MA, klurie@wpi.edu

the most practical way towards it will be a *material switching*, i.e., a transfer from one material to another implemented by suitable technical means whenever and wherever necessary.

This transfer is accompanied by the energy flux brought into the system (or released from it) by an external agent. When we work with DM, the presence of an external agent is both inevitable and critical: it serves as a necessary link with the environment, maintaining the dynamic nature of a material formation.

Once implemented, DM offer a diversity of effects unthinkable with ordinary materials, among them efficient ways to control wave propagation and, in particular, introduce a novel principle of *power generation, transport, and storage of energy*. DM are also of universal significance for optimization because they may be adjusted to fit the environment changing in space and time and therefore offer a great amount of resources never stored in ordinary materials. In this capacity, they represent a natural material arena for the purposes addressed in dynamics.

These ideas belong with a core of material science today; they can be realized and verified by building dynamic materials structured as large arrays (transmission lines) of coupled and actively controlled oscillatory elements. One could use for this purpose the *LC-cells* in the electromagnetic implementation, and the mass-spring elements in mechanical implementation; in either case, the material parameters of the elements are subjected to active control by an external agent. The wave propagation along the DM arrays presents a number of distinguishing features. As demonstrated by theoretical analysis, immediate consequences of that will be the ability of such structures to **dynamically amplify, tune, and compress travelling disturbances, as well as store them, over a wide range of carrier frequencies**. Once the typical space and time scales of microfabricated elements are significantly smaller than the spatial wavelength and the temporal period of the disturbance, these structures can be effectively considered as continuous dynamic materials.

This paper offers a fabrication oriented design of a device accumulating and storing the electromagnetic energy in travelling RF-waves. The device represents a transmission line controlled by an external energy source that maintains a checkerboard material geometry in space-time.

We first describe the basic principles and provide a mathematical formulation. In subsequent sections, an engineering realization is described at some length, by using the parts currently available from the market. The robustness of the device as well as its effectiveness, with account of unavoidable losses and parasite effects, is given a numerical evaluation.

3 General Principles of Power Generation and Energy Storage in DM structures

Below follows an example of a dynamic material that illustrates some of their special features. Specifically, it demonstrates how proper control over travelling waves may produce a new mechanism of **power generation and power storage incorporated in the same device**.

Assume that we have two conventional isotropic dielectrics: material 1 and material 2, with the wave impedance $\gamma = \sqrt{\mu/\epsilon}$ and phase velocity $a = 1/\sqrt{\mu\epsilon}$ taking values (γ_1, a_1) and (γ_2, a_2), respectively.

Assume that $\gamma_1 = \gamma_2$ and $a_2 > a_1$, so the wave impedances match, and the material 2(1) is "fast" ("slow"). Consider a periodic material laminate in 1D-space and time, with materials 1(2) occupying the alternating layers with volume fractions $m_1(m_2)$ in every period. The laminate will be called static (temporal) if the layers go perpendicular to the z-axis (t-axis). A static laminate is an ordinary material assemblage in space, while a temporal laminate is already a DM produced by a temporal property switching. A plane electromagnetic wave travelling through the laminate in z-direction exhibits no reflection on the material interfaces in both static and temporal versions [9], [2], [10], [11], [13]. When the wave travels through a static laminate, its energy remains constant in time. When the wave travels through a temporal laminate, its energy increases by the factor a_2/a_1 each time the wave enters "fast" material 2 from "slow" material 1, and decreases by the factor a_1/a_2 when it leaves material 2 and enters material 1. The net energy gain over a temporal period is therefore zero. **The energy gain (loss) occurs due to the work pumped into the wave (or taken out of it) by an external agent that changes the material properties at each temporal property switching**.

We desire to accumulate energy in a travelling wave; with this goal in mind, laminates are not a solution. To guarantee accumulation, we have to avoid the moments of energy loss by finding some other way for the wave to

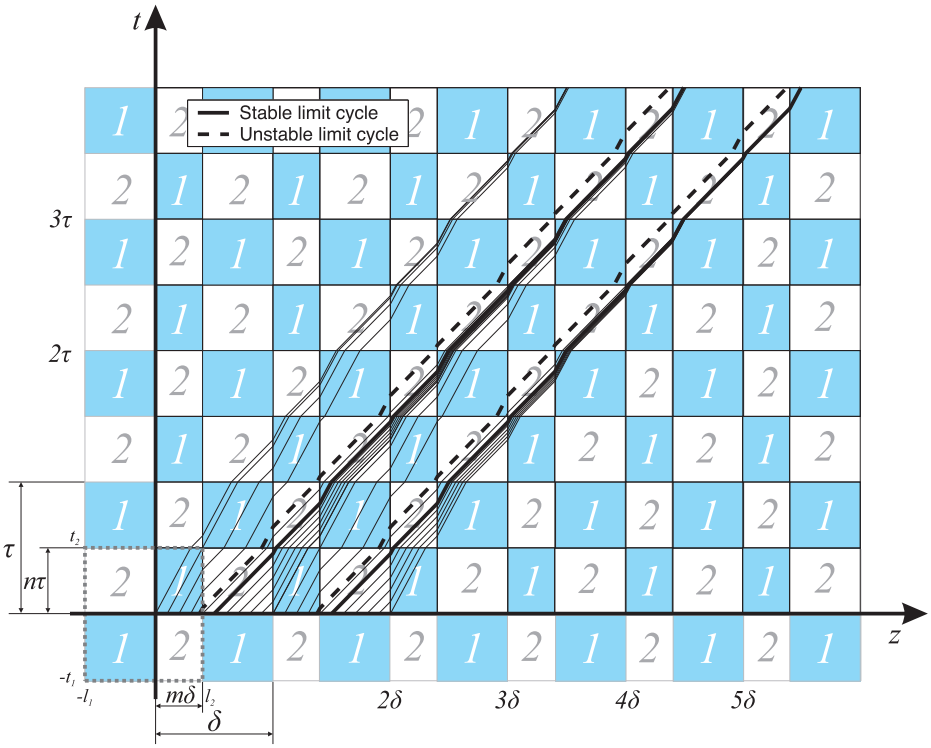

Figure 1: A checkerboard structure in space-time with wave routes and limit cycles for $a_1 = 0.6, a_2 = 1.1, m = 0.4$ and $n = 0.5$

enter the "slow" material 1. This way may be the one across the spatial, instead of temporal, interface, because when the wave crosses a spatial interface it doesnt lose energy since the energy flux remains continuous. We arrive at the idea of testing **a rectangular material structure in space-time as a possible energy accumulator, because it offers both spatial and temporal interfaces**. Specifically we try a "checkerboard" structure shown in Figure 1. This is a double periodic structure in (z, t)-plane, with periods δ and τ, in z and t, respectively. It can be implemented as a static periodic laminate, with period δ, existing from $t = 0$ to $t = n\tau$ (see Fig. 1), at which point its material properties "flip over", so that where there was material 1 there now appears material 2, and *vice-versa*. This pattern is maintained from $t = n\tau$ to $t = \tau$, and the procedure repeats periodically in time, with period τ . Parameters m and n denote the fraction of material 1 in the periods δ and τ . We expect that this structure will be able to support the wave routes with no energy loss.

A remarkable property of the checkerboard consists in its ability to meet these expectations. We see in Figure 1, that the wave enters the "fast" material 2 across the temporal interfaces where the wave gains energy, and leaves it (i.e., enters material 1) across the spatial interface where no energy loss occurs. The waves travel with no reflections, and consequently the system is not oscillatory and requires no frequency adjustment. So the phenomenon of energy accumulation stays in effect for all frequencies. Also, the accumulation is robust because it occurs in some continuous intervals of parameters a_1, a_2, m, and n; particularly their values related to Figure 1 fall into such intervals (in [10], there are given **sharp bounds** for such intervals, and their attainability is confirmed numerically (so called "plateau effect")). The waves come into distinct groups that approach some selected characteristics - *the limit cycles*. Energy is accumulated in these groups in the form of narrow pulses that carry high power. The cycles are stable, because they attract the neighboring wave routes. In Figure 1 we have one stable (boldface curve) limit cycle per period; any two consecutive stable limit cycles are separated by an unstable limit cycle (dashed curve) that repels the neighboring characteristics. For one period, the energy of the wave increases by a factor $(a_2/a_1)^2$ because it is pumped twice into the wave; as a result, **the energy of the wave grows exponentially in time**.

The DM checkerboard may be miniaturized by placing two mirrors (ideal reflectors) at the opposite ends of the

spatial interval occupied by the system. Reflected waves are amplified as they travel through the checkerboard DM in opposite directions. This will cause nonstop amplification as the waves travel back and forth. When the energy supply from an external agent stops, the temporal switches are no longer maintained, and the system becomes a static laminate serving as a battery storing the energy already accumulated in the waves that still continue travelling between the mirrors but with no energy gain.

4 Mathematical Formulation

Consider a plane electromagnetic wave propagating along the z-axis; for such a wave, the electromagnetic field $\mathbf{E}, \mathbf{B}, \mathbf{D}, \mathbf{H}$ is defined as

$$\mathbf{E} = E\mathbf{j}, \;\; \mathbf{B} = B\mathbf{i}, \;\; \mathbf{H} = H\mathbf{i}, \;\; \mathbf{D} = D\mathbf{j}, \tag{1}$$

and the Maxwell's equations take the form

$$E_z = B_t, \;\; H_z = D_t, \tag{2}$$

with

$$\mathbf{D} = \epsilon\mathbf{E}, \quad \mathbf{B} = \mu\mathbf{H}. \tag{3}$$

We assume that ϵ, μ, termed, respectively, the dielectric permittivity and the magnetic permeability of a material, as well as, E, B, D, H, depend on z, t. As mentioned in section 2, we allow for two immovable material constituents: material 1 with properties ϵ_1, μ_1, and material 2 with properties ϵ_2, μ_2. Below we use, instead of ϵ and μ, an alternative pair of material parameters: the wave impedance

$$\gamma = \sqrt{\mu/\epsilon}, \tag{4}$$

and the phase velocity

$$a = 1/\sqrt{\mu\epsilon}. \tag{5}$$

Assume that $\gamma_1 = \gamma_2 = \gamma$ and $a_2 > a_1$, so the wave impedances match, and the material 2(1) is "fast" ("slow"). Eqs.(2) are satisfied if E, B, D, H are expressed through potentials u, v by setting

$$E = u_t, \;\; B = u_z, \;\; H = v_t, \;\; D = v_z. \tag{6}$$

Eqs.(3) are then reduced to

$$R_t + aR_z = 0, \quad L_t - aL_z = 0, \tag{7}$$

where

$$R = u - \gamma v, \quad L = u + \gamma v \tag{8}$$

are the Riemann invariants related to the right- and left-going waves, respectively.

Below we discuss the wave propagation through a checkerboard structure introduced in section 2. Along the static interfaces $z = const$, we require continuity of E and H, i.e., of u and v. Along the temporal interfaces $t = const$, B and D should be continuous, which, again, is equivalent to the continuity of u and v. So, these variables should be continuous across any interface in a checkerboard; an alternative will be the continuity of Riemann invariants R and L.

The wave propagation along z-axis can be imitated in a transmission line assembled from the *LC-cells*, with the material switching in space-time from L_1, C_1 to L_2, C_2, and *vice versa*, in each cell (Fig. 2); we will use the same symbols to designate the *linear* inductance and capacitance in the line.

The equations governing the voltage V, magnetic flux Φ, the charge Q, and the current I, are identical with (2) and (3), with substitutions

$$E \to V, \quad B \to \Phi, \quad D \to Q, \quad H \to I, \tag{9}$$

and

$$\epsilon \to C, \quad \mu \to L. \tag{10}$$

The energy accumulation occurring at the moments of temporal switching in a properly designed checkerboard (see section 2) appears to be a direct consequence of Eqs.[2], [3], or their transmission line counterparts.

In the following sections, we discuss an attempt to produce a reasonable engineering design of a material LC-assembly that maintains a checkerboard property pattern in space-time and demonstrates the special effects. This effort had to overcome several technical difficulties listed below:

A) The model used very large number of L and C components - almost 6000 of each, which will lead to prohibitively expensive (and large, among other issues) implementation.

B) Although the values of L were reasonable to achieve, the values of C were so low that no physical device could reliably reproduce it in large numbers.

C) All components in the model were ideal, that is, not only they didn't represent any actual physical parts, but they also didn't account for such things as losses, parasitic and other effects that real parts would have.

D) It remained unclear how temporal changing of the values of C and L would be done in practical implementation.

We split the analysis into two consecutive stages.

5 Material Design: Stage 1

The goal of Stage 1 is to deal with issues A and B: still using ideal components, find a solution that contains reasonable amount of parts, while still demonstrating the desired effect. All simulation for this Stage was done in OrCAD Pspice (Cadence), which is more powerful and flexible than LTspice. The ideal L and C components were re-created in OrCAD and a circuit consisting of two identical media was constructed (the term medium refers to a transmission line simulated with a limited number of lumped LC-circuits). Since OrCAD allows creation of hierarchical designs, it is fairly easy to change the amount of LC-circuits in a medium for a different simulation run.

One of the reasons for the very large number of LC-circuits is that the design was assumed to be a linear assembly of LC-cells: many media were connected in series, forming a long chain, where the initial pulse entered the first medium, travelled through all connected media in sequence, and left the last medium at the end. In this design, the vast majority of the LC-elements (referred to as "LC-cells" from now on) are idle at any given time, since the pulse energy is present only in one of the many media. This also led to very long simulation time - although mostly idle, all of the nodes and elements in the system still need to be simulated and computed.

The first attempt to solve this problem was to make the media work more than once in a single run, that is, for spatial switching, use the same medium over and over again. To accomplish this, a circular pattern was created in the following manner: the two media are connected in series; the initial pulse enters the first medium; as soon as the pulse is contained entirely within the first medium, the input to this medium is disconnected from the pulse source and connected to the output of the second medium, thus forming a loop; the pulse will then experience spatial switching between the two media indefinitely (in theory, of course).

This approach required that the entire pulse has to fit in the medium as it travels across, so that the medium temporal switching can occur at that exact moment. Also, the number of LC-cells may be cut in half (with the same result) if we notice that when a transmission line is shorted at its end, the total reflection of the incident wave occurs. The reflected wave will have opposite polarity and travel in the opposite direction. In the underlying theory it does not matter what direction of travel and what polarity the pulse has to be for the energy accumulation to work, as long as the temporal property switchings of the mediums occur at the right times.

Fig. 2 shows the overall schematics of such an arrangement; here, each of the two mediums consists of 32 LC-cells. The initial pulse source, ABM3, is connected to terminal 1 of the first medium; the terminal 2 of the second medium is shorted to ground. It is worth noting that after generating the initial pulse, the output voltage

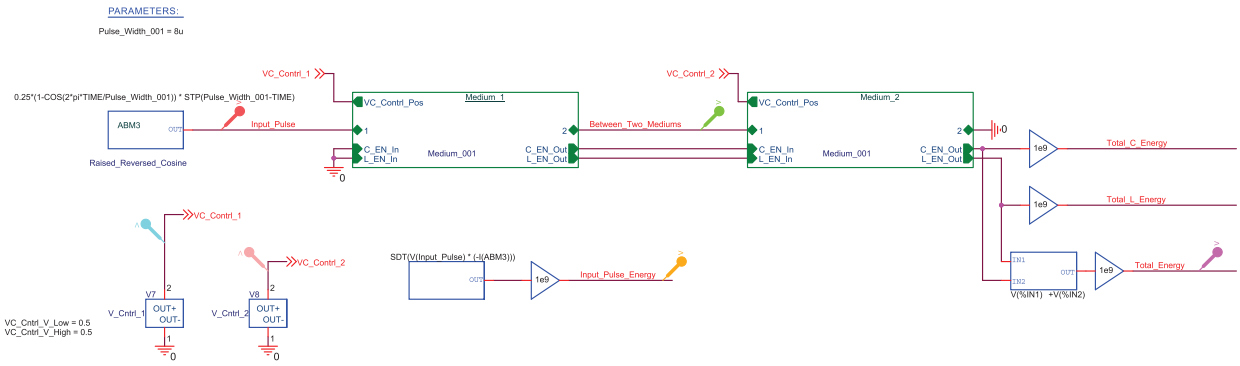

Figure 2: Overall schematics of the LC arrangement (ideal elements)

of ABM3 is held at the ground level, hence the terminal 1 of the first medium is automatically shorted to ground for the rest of the simulation. On the schematics there are also some additional elements that control temporal switching of the mediums (VC Contrl 1 and VC Contrl 2), as well as elements for calculating total energy contained within the system.

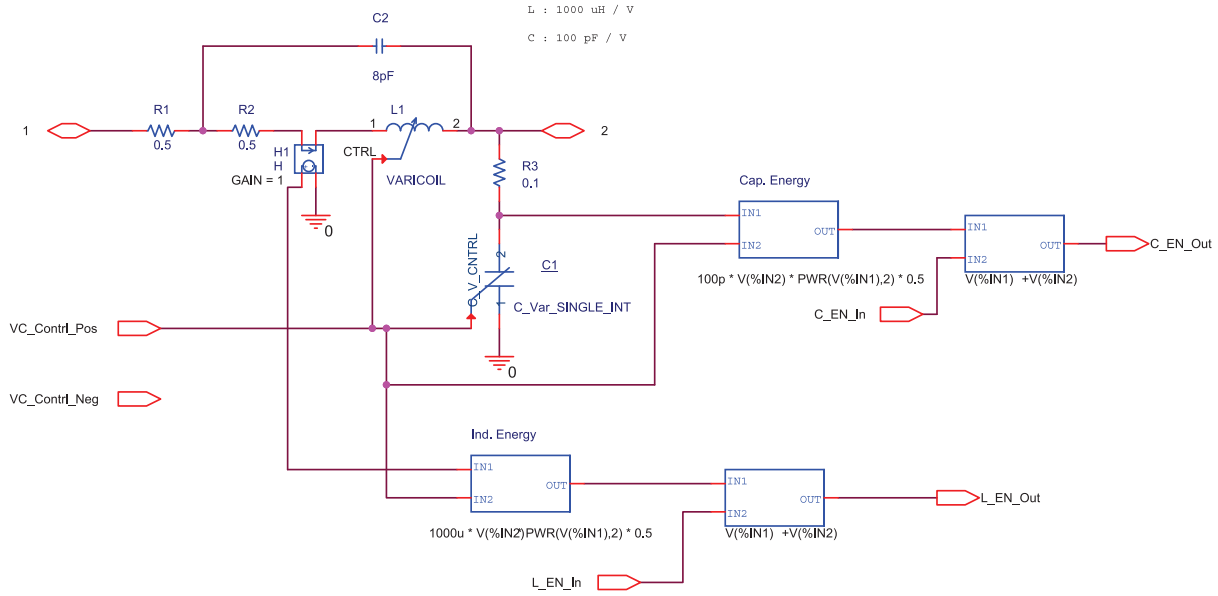

Figure 3: Schematics of an individual LC-cell (ideal elements)

Fig. 3 shows an individual LC-cell. Besides the actual ideal variable L and C components ($L1$ and $C1$) it contains some parasitic components as well (the values were chosen so that they are reasonably close to what might be encountered in the real $L1$ and $C1$ with the chosen values and within the frequency range of interest). $C2$ represents parasitic capacitance of $L1$; the parasitic inductance of $C1$ is negligible in our case, and therefore omitted. $R1$, $R2$ and $R3$ represent series resistances of $L1$ and $C1$ to account for losses in these elements. It also contains additional components that allow for calculation of instantaneous energy contained in $L1$ and $C1$.

The system without temporal switching was first examined (only spatial switching occurs). This simulation is useful in observing how the initial pulse travels through both media (that are exactly the same in this case) multiple times, how it "distorts" due to limited "bandwidth" of the media, and how it decays due to the losses in parasitics. Of course, without temporal switching there is no "energy accumulation". Results of this simulation are shown in Fig. 4. The names of the traces match the names of nodes on the schematics. The horizontal axis represents simulation time in microseconds (μs).

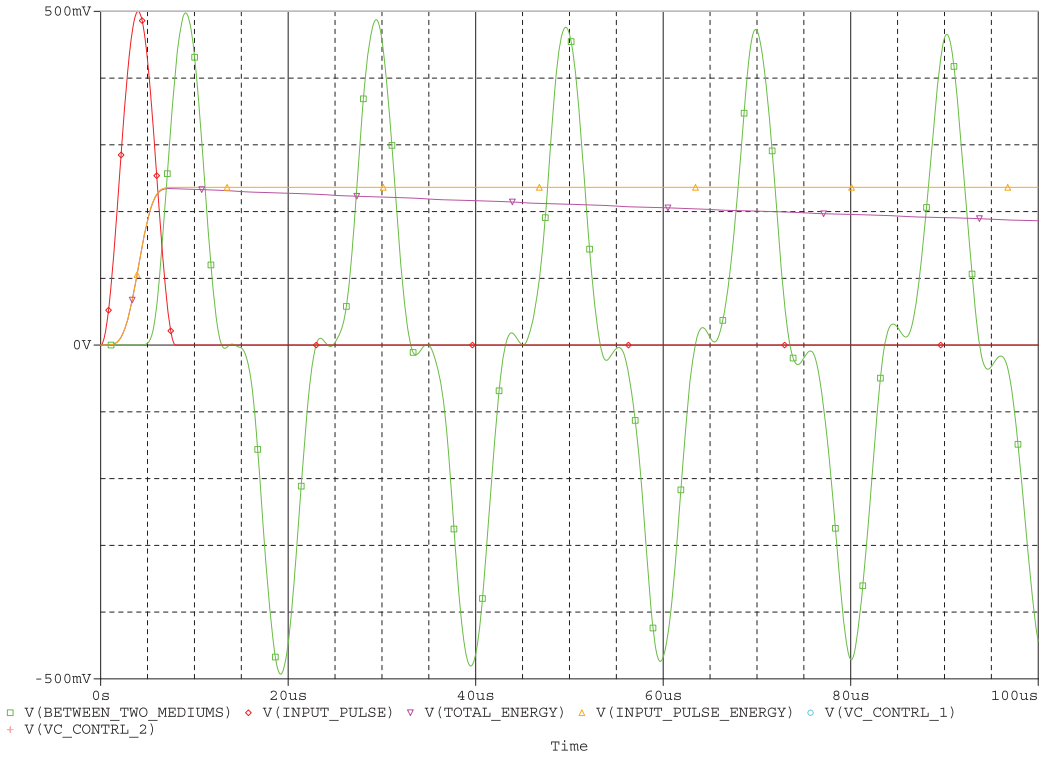

Figure 4: A pulse propagation through a "loop" combined from two media alternating in space

The red trace shows the initial pulse as it enters the first medium. The green trace shows the waveform observed at the point between the two media (the same green color used on all subsequent graphs as well); the positive pulses propagate from left to right (according to the schematics view), and the negative ones travel from right to left. The results in Fig. 4 show that the initial pulse, after 9 passes through the media, retains its shape reasonably well, showing only a slight distortion and decay. The energy of the initial pulse is shown in dashed orange trace. The trace for the total energy contained within the system (purple trace) shows a linear decline (as should be expected) from initial value of ≈ 0.23 to ≈ 0.19 at the end ($\approx 17\%$ decline; values are relative). Although the vertical axis is shown in mV (millivolts), for energy traces it is in relative joules.

The system might appear to be of a resonant nature as the pulse travels back and forth fully reflecting from both ends, creating an appearance of a resonator. However, this is not the case. The pulse width is smaller than the size of the resonator, and reflection off of one end does not affect reflection off the other. This system behaves exactly the same as a linear one with many media and no reflections at all; the only difference is that here the media get reused many times over.

One interesting observation that was not obvious at the outset is that if the initial pulse is symmetrical around its middle point (which it is in our case), after reflection from a shorted end, there is a point in time where the energy contained within all capacitors is equal to zero (which means that voltages across all capacitors are all equal to zero). This corresponds to the time when exactly half of the pulse is reflected from the shorted end, and since the reflected half is exactly the same as the incoming half but in opposite polarity, they cancel each other.

In Fig. 5, blue trace shows the total energy stored in all capacitors in the system according to the formula: $E_c = \Sigma_{k=1}^{n}(C_k * U_{C_k}^2/2)$, where k is sequential number of an LC-cell, U_{C_k} is the voltage across capacitor in that LC-cell, and n is the total number of LC-cells in the system. The times when E_c is equal to zero correspond to the moments when the pulse energy is contained entirely within one of the two media one half incoming and the other half reflected. This provides for convenient way to determine the exact timing for temporal switching of the media. For a reference, the red trace shows the total energy stored in all inductors in the system: $E_L = \Sigma_{k=1}^{n}(L_k * I_{L_k}^2/2)$. As in the previous Figure, purple trace represents the total energy.

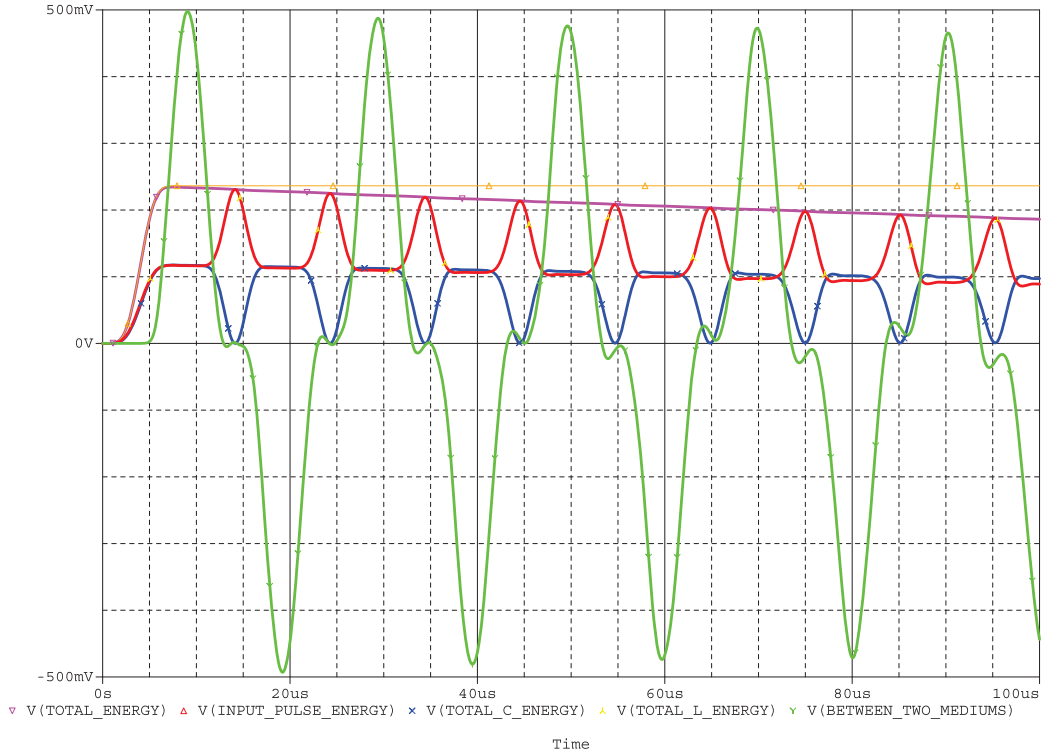

Figure 5: Energy stored in capacitors in the absence of temporal switchings

It is worth mentioning here that there is a different termination method for the media that we could have used - rather than shorting the ends, leave them unconnected (floating). In this case there will still be a total reflection from the ends, but without voltage phase reversal (there will be, of course, current phase reversal instead). The boundary condition will change from $V = 0$ to $I = 0$, and that means that the same zeroes will occur in inductor currents, rather than in capacitor voltages. This observation may be beneficial for Stage 2, when we will have to find a real solution for temporal switching.

Using "zeroes" in capacitor voltages as reference points, the timing of the control signals was specified so that the temporal switching does not happen when the spatial does, and *vice versa*, and the result is shown on Fig. 6. Here, the temporal switching does occur, and the values of the L and C are determined by the magnitudes of $VC_{Contrl1}$ (for medium 1) and $VC_{Contrl2}$ (for medium 2) as blue and red traces. The values of the capacitors are defined as $C = VC_{Contrl} * 100pF$, and inductors as $L = VC_{Contrl} * 1000\mu H$. The scaling was chosen for convenience of simulations and for better displaying the control voltages on the same graph with other traces. In Fig. 6, the control voltages change from 0.45V to 0.55V and back, which correspond to $L : C$-pairs switching from $45pF : 450\mu H$ to $55pF : 550\mu H$.

Since both L and C change their values proportionally together, the "characteristic impedance" of the media remains the same (disregarding losses): $\gamma = \sqrt{\frac{L}{C}} = \sqrt{\frac{450*10^{-6}}{45*10^{-12}}} = \sqrt{\frac{550*10^{-6}}{55*10^{-12}}} \approx 3,160Ohms$. However, the "phase velocity", $a = \frac{1}{\sqrt{LC}}$, does change between the values of $a_{slow} = \frac{1}{\sqrt{550*10^{-6}*55*10^{-12}}} \approx 5.75 * 10^6$ and $a_{fast} = \frac{1}{\sqrt{450*10^{-6}*45*10^{-12}}} \approx 7.03 * 10^6$. The absolute values of phase velocity do not have any physical meaning (as in meters/second) in our case (we just model a transmission line with lumped components, which may be large or small, as well as spaced apart differently, but electrically still being the same) and do not really matter. The parameter of interest here is the ratio between the two values, which determines the "energy accumulation" factor. In simulation on Fig. 6 it is $7.03/5.75 \approx 1.22$.

There were eight temporal switchings in Fig. 6, so the total energy accumulation should amount to $\approx 1.22^8 \approx 4.9$. The total energy trace (purple), at the end of the graph, shows the value of ≈ 0.94. As we recall from Fig. 5, the initial pulse energy without temporal switching had been reduced to ≈ 0.19 due to losses. That gives us

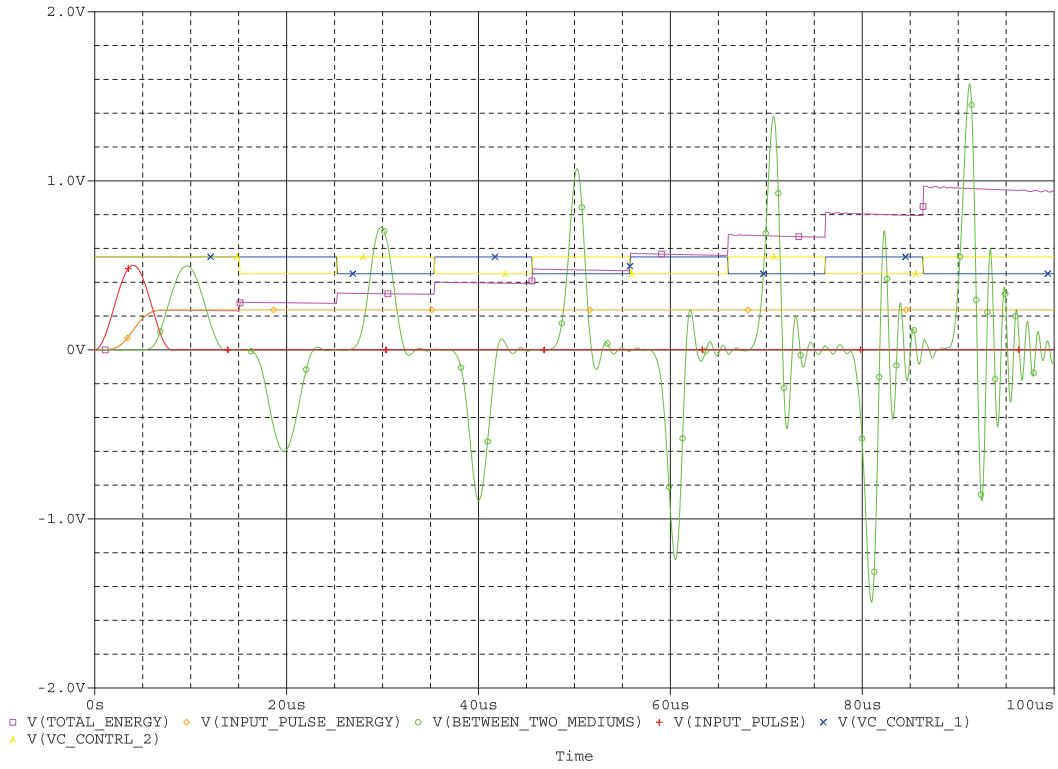

Figure 6: Evolution of pulses in the presence of temporal switchings

total accumulation of $0.94/0.19 \approx 4.95$, which is very close to the expected value of 4.9 (which, actually should be ≈ 4.98 if we increase precision of the above calculations).

The total energy accumulation matches very well with theory predictions. So does the overall pulse shape: the amplitude increases and the width narrows. However, the pulse exhibits some secondary oscillations that grow with each spatial and temporal switching (unlike in Fig. 4, where there is virtually no oscillations throughout the simulation). This is due to a limited bandwidth of the lumped-components nature of the media. The initial pulse shape was chosen to contain as little high-frequency spectrum components as possible (for a given pulse width) – numerous profiles were simulated and chosen the raised-inversed cosine as the best in this regard. But shaping of the pulse due to the energy accumulation (desired effect) causes the spectrum to contain more and more high-frequency components that lead to oscillations and distortions (undesired effect).

These distortions may not present a problem since it is understood that this is just a realistic approximation of a theoretical principle. However, it is desirable to reduce them as much as possible. One possible solution lies in the fact that energy accumulation is proportional to the ratio of a_{fast}/a_{slow}. If we increase this ratio, we would need fewer temporal and spatial switching to achieve the same overall gain.

Fig. 7 shows what happens with the increased energy gain. Here, everything is the same as in Fig. 6 except that the control voltages switch between $0.4V$ to $0.6V$, which corresponds to $a_{fast}/a_{slow} = 1.5$. After just four temporal switching (at $\approx 50\mu s$), the total energy reaches ≈ 1.06 compared with ≈ 0.21 at the same moment in Fig. 4 - gain of ≈ 5.05 (theoretical gain is $\approx 1.5^4 \approx 5.06$). Not only the energy accumulation is larger here, but the pulse shape at this point is better than that at the end of simulation in Fig. 6. After the fifth temporal switching in Fig. 7 (at $\approx 56\mu s$), however, the pulse shape deteriorates rapidly, and by the end of the simulation it is hard to see the where the pulse is in between the oscillations.

To summarize, the results of Stage 1 reduce to the following.

1. It is possible to demonstrate the principle of energy accumulation with a reasonable number of ideal LC-cells (even with a close-to-real losses and parasitics present).

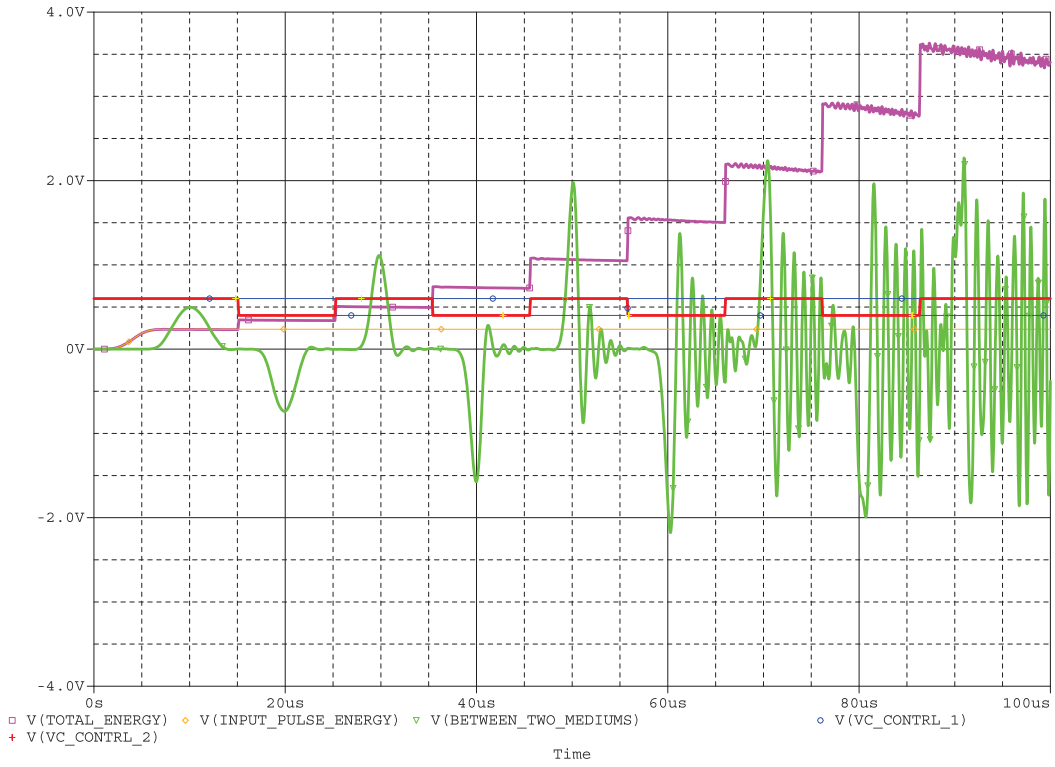

Figure 7: Progressive energy accumulation in pulses travelling through a DM checkerboard assembly

2. It is going to be a trade-off between the a_{fast}/a_{slow} value and the number of spatial and temporal switchings, depending on the requirements for the end customer.

3. While energy accumulation is clearly seen in all of the simulations, it is just a "convenience" of numerical simulation. In real circuitry, the pulse shape can be observed with an oscilloscope, but it is unclear how to characterize the energy gain so it is obvious to a casual observer.

6 Material Design: Stage 2

In Stage 1, it has been demonstrated, by means of Pspice simulation, that there may be a viable solution to practical implementation of a circuit, that is, the issues A and B have been resolved. This Stage 2 deals with issues C and D, which are:

C) All components in the model were ideal, that is, not only they didn't represent any actual physical parts, but they also didn't account for such things as losses, parasitic and other effects that real parts would have.

D) It remained unclear how temporal changing of the values of C and L would be done in practical implementation.

Before we model the system with "actual" L and C components, we have to select them first. These components have to be capable of temporal change in their values in a controlled manner. It is quite easy for the C components: we can use readily available variable capacitance diodes, i.e., varicaps or varactors. They are semiconductor diodes specifically manufactured so that their reverse-biased capacitance is not only well defined, but also changes significantly with applied voltage. There are many types available on the market from various manufacturers. Their primary use is in RF circuits for frequency tuning, and the absolute capacitance values are generally in the $\approx 10pF \approx 100pF$ range (with that in mind the values of the "ideal" capacitors were chosen for Stage 1 simulations).

Inductor choices, on the other hand, are not that obvious. There are plenty of inductors available for various

purposes; however, the vast majority of them are designed with the goal of maintaining L-value at a constant level under all operating conditions - quite opposite to ours. There are also a limited number of inductors for "niche" applications, such as magnetic amplifiers which change their L-value abruptly when current through them reaches certain level. These inductors tend to be targeted for high power electronics (e.g., power supplies); they are very limited in choice and bulky. Also, it will be difficult to control their L-value since it changes too substantially with a little change in the current. Even if it were possible to control these devices, it is not clear how it can be accomplished in practice, since the inductors are not ground-referenced like the capacitors but rather connected in series with each other.

Other approaches were also considered. One of them was the possibility to use gyrators: active circuits (consisting of operational amplifiers, resistors and capacitors) that mimic behavior of real inductances according to the general formula $I = \frac{1}{L}\int V dt$. This approach was dismissed due to two factors:
a) while single gyrator circuits are generally stable when component values are chosen right, many gyrators connected together might not be stable at all, and,
b) presence of amplifiers (or any active components, for that matter) in the media might give an impression that it is these components that are responsible for the energy gain, and not the underlying principle under study here.

Another possibility considered was the use of inductors with multiple windings (transformers), where currents through one or more windings control inductance in another winding (since control currents change permeability of the core material). However, these transformers are not designed for this particular purpose, and, like regular inductors, maintain their L-value within wide range of currents. Manufacturing specialized transformers with specifications tailored for this project would be cost prohibitive.

However, the solution for temporal switching of inductors was hinted at in Section 4. It was noted that if the initial pulse is symmetrical around its middle point and a total reflection occurs at an open medium's end, there is a point in time when all currents through all inductors will be equal to zero. This is exactly the time when temporal switching should take place, since all of the pulse energy is contained within the medium. Since at this time there is no energy stored in the inductors ($E = \frac{L*I^2}{2}$), rather than trying to change the value of an inductor itself, we can add (or subtract) another inductor of a fixed value so that total inductance changes to a pre-determined value. The principle of conservation of magnetic flux is satisfied, since it remains the same (zero) before and after temporal switching. The same is true when this switching occurs in the "empty" medium for the same reason. When temporal switchings occur, all energy accumulation is due to capacitors change in value; the only role of the inductors switching is to maintain the same characteristic impedance of the media.

When two inductors are connected in series, the total inductance is the sum of the two: $L_{TOT} = L1 + L2$ (assuming there is no magnetic coupling between the two inductors). So, if we have a switch across $L2$ that opens and closes at appropriate times, the total inductance will change from $L1$ when switch is closed ($L2$ is shorted), to $L1 + L2$ when the switch is open. This is the solution that was chosen to be implemented in practice, since it requires just two small, off-the-shelf inductors and a simple switch. The only disadvantage of this approach is that once the values of the inductors are chosen and they are physically installed on a board, they cannot be easily changed (e.g., for a different value ratio). This limitation was not considered significant enough for this study, since the goal here is to demonstrate the principle, not to engage in detailed studies of effects of various values on the outcome.

So, for Stage 2, the configuration of the media were changed from "shorted ends" to "floating ends" (see Fig. 8). Here, the sequence of events is as follows:

a) The initial pulse is generated and enters the first medium at the left (as seen on the schematics); when the pulse has entered the media completely, the pulse source is disconnected from the first medium, thus leaving this node floating for the rest of the simulation.

b) The right side of the second medium is floating as well, for now.

c) The simulation is run for a given number of reflections off of both floating ends of the media.

d) After a given number of temporal and spatial switchings, the right side of the second medium is connected to a load resistor with the same value as the characteristic impedance of the media, thus "dumping" the accumulated

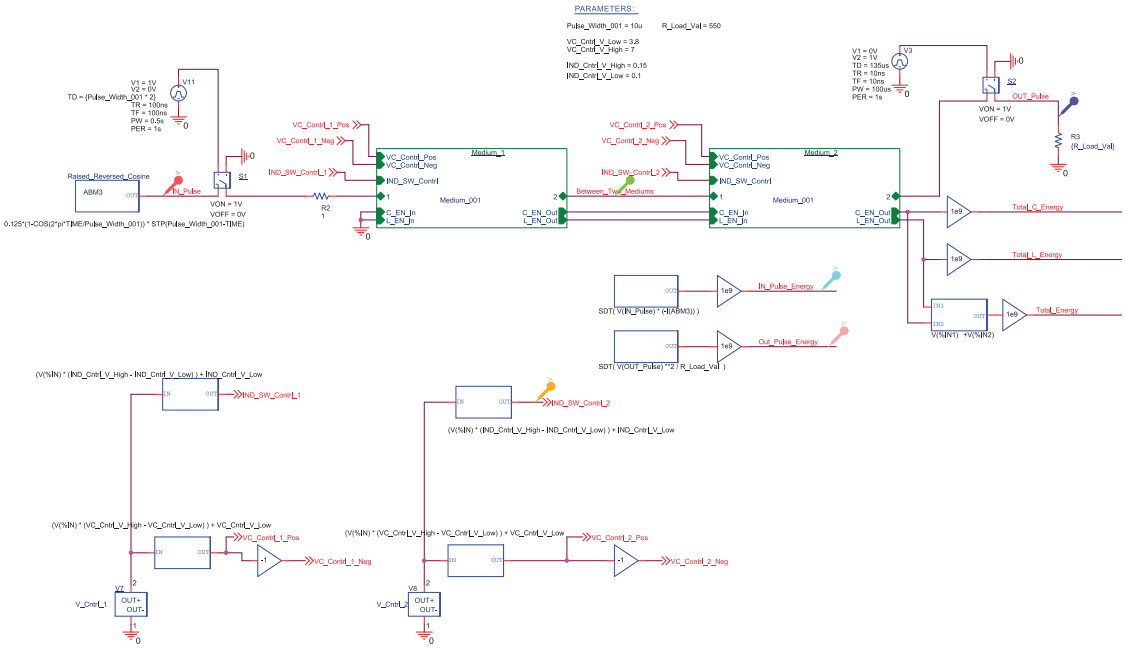

Figure 8: Overall schematics of the LC arrangement (real elements)

energy into this resistor.

Initial attempt was made using real components with values close to those used in Stage 1 with ideal ones. However, after running simulations with these values it became obvious that losses in the LC-cells (there are 32 of them in each of the two media) outweighed the energy gain from temporal switchings: the amplitude of the pulses had been diminishing over time instead of increasing.

After analyzing these results it became clear that majority of the losses occur in inductors (there are very little losses associated with varactors at our frequencies, voltages and currents - simulations done with "ideal" inductors and "real" varactors show virtually no energy losses). Generally, inductors with larger L-values tend to have larger parasitic properties primarily due to longer windings and/or higher core material volume. So, a logical path to try to remedy large losses is to decrease the values of inductors. To maintain timing of the system (i.e. to try not to affect the "phase velocity"), values of the capacitors will have to increase proportionally, which is not a problem for an implementation in a real system: we can connect multiple varactors in parallel to achieve desired value. Varactors are small and inexpensive devices, and increasing quantity of them in the system will not be detrimental to the size and the cost of the implementation.

Multiple simulations were run with choice of inductors with lower L-value and a corresponding increase in number of varactors. The results, indeed, showed that system performance improved significantly as the inductors L-value decreased. The final choice of the LC-cells was based on the trade-off between performance and number of varactors in each cell.

Fig. 9 shows the schematics of the individual LC-cells. Now, instead of ideal variable L and C components, they contain "real" components $L1$ and $L2$ with a switch $S1$ for "variable inductors", and $D1 - D4$ for varactors (each of which consists of two varactors with a common cathode for a total of eight). The passive components that were present in "ideal" simulation to account for "reasonable" losses were removed, since now we have "real" $L - C$ components with losses represented within their corresponding Pspise models. And as before, there are also additional, purely mathematical, components that allow for calculation of instantaneous energy contained within the LC-cells. On the LC-cells schematics there are also two passive elements: resistor $R4$ and diode $D5$. Their presence warrants some additional explanation. As it was discussed in Stage 1, when a pulse reflects off of a shorted end of a medium, the reflected pulse will have opposite polarity from an "incoming" one (voltage-wise). In the opposite case, when reflection occurs from an open end, the polarity will remain the same (this is the case

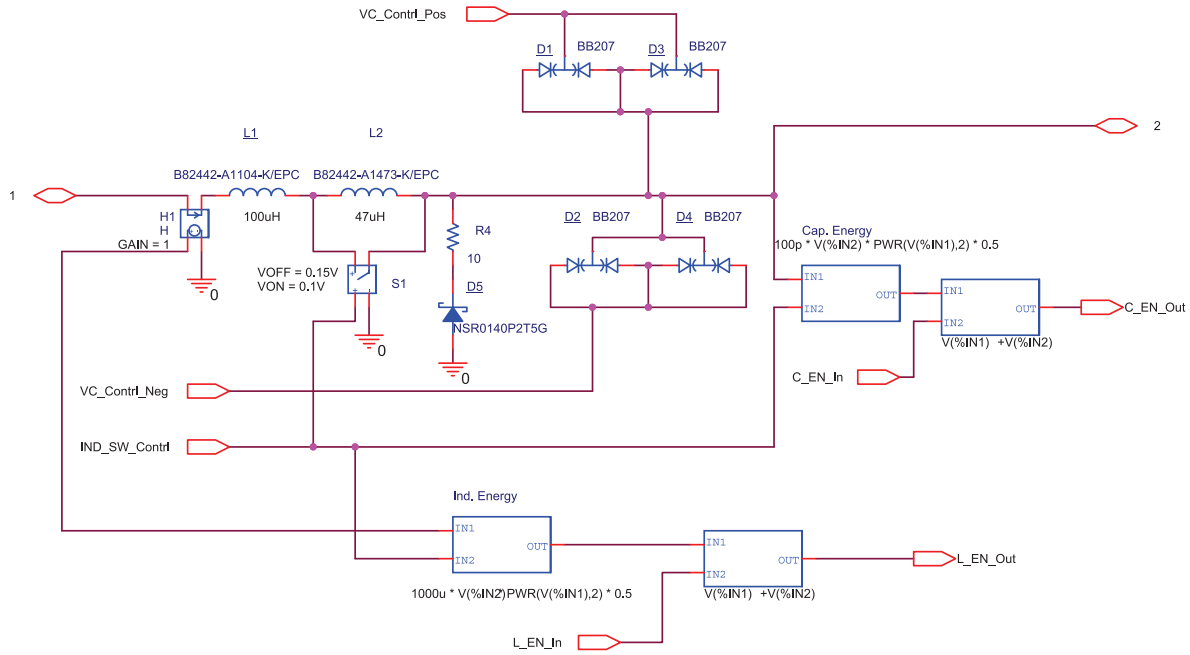

Figure 9: Schematics of an individual LC-cell (real elements)

at this Stage). Since our initial pulse has positive polarity, then, in theory, it will remain positive throughout the entire experiment. However, as was seen in Stage 1, distortions and oscillations cause spikes in voltages that go in the opposite polarity. The presence of $R4$ and $D5$ does not allow these spikes to go in the negative polarity, thus preventing the distortions to grow more and more as the energy amplification takes place. Of course, this "clipping" wastes some of the energy in the system, but it helps in preserving the pulse shape in exchange.

As seen on the LC-cells schematics, the values of inductors are $100\mu H$ and $47\mu H$, which gives the ratio of $\frac{L1+L2}{L1} = 147/100 = 1.47$. To match this ratio on the varactor side (to maintain the same characteristic impedance of the media), the control voltages were chosen so that capacitance alternates between $30pF$ and $45pF$ for each of the varactors. This corresponds to control voltages being $7V$ and $3.8V$, respectively. Since there are eight varactors connected in parallel in each cell, the total capacitance alternates between $240pF$ and $360pF$ for the ratio of 1.5. An important note regarding simulations with "real" parts: while in simulations with "ideal" components (as in Stage 1) we can control all parameters (including values of L and C) exactly, this is not the case with real parts. Real parts have nominal values, usually measured at certain conditions; depending on stated tolerances, actual values will vary from part to part. In addition, the values themselves depend on other factors such as currents, voltages, frequency of interest, etc. As such, all values that pertain to real parts should be treated as approximate.

The multiple simulations were run with the parameters outlined above, with varying amplitude of the initial pulse. The result of one of them is shown on Fig. 10 (others looked similar). Here, red trace is the initial pulse, teal is the initial pulse's energy, green is the voltage observed between the two media as the pulse travels back and forth, orange is one of the control voltages (to show when temporal switchings occur), blue is the voltage of the output pulse (as it is being dumped into the load resistor), and pink is the total energy out of the system.

Results of these simulations are summarized in Table 1. In all cases, the initial pulse shape was one full period of inversed-raised cosine with width of $10\mu s$; each of the two media contained 32 LC-cells, and characteristic impedance of the media was approximately $640Ohms$.

The Table shows that, after 10 temporal switchings, the overall energy gain is as high as 9.8. This means that, on average, each temporal switching creates $\sqrt[10]{9.8} \approx 1.26$ times energy gain. This is pretty good compared to "ideal", "lossless" value of ≈ 1.5. It is worth noting here that even small reduction in gain (due to losses and other factors) at each switching will lead to a large reduction in overall result (compare 9.8 times to a "theoretical" gain of $1.5^{10} \approx 58$). It does not mean, of course, that the overall system efficiency is $9.8/58 \approx 17\%$. It is also not

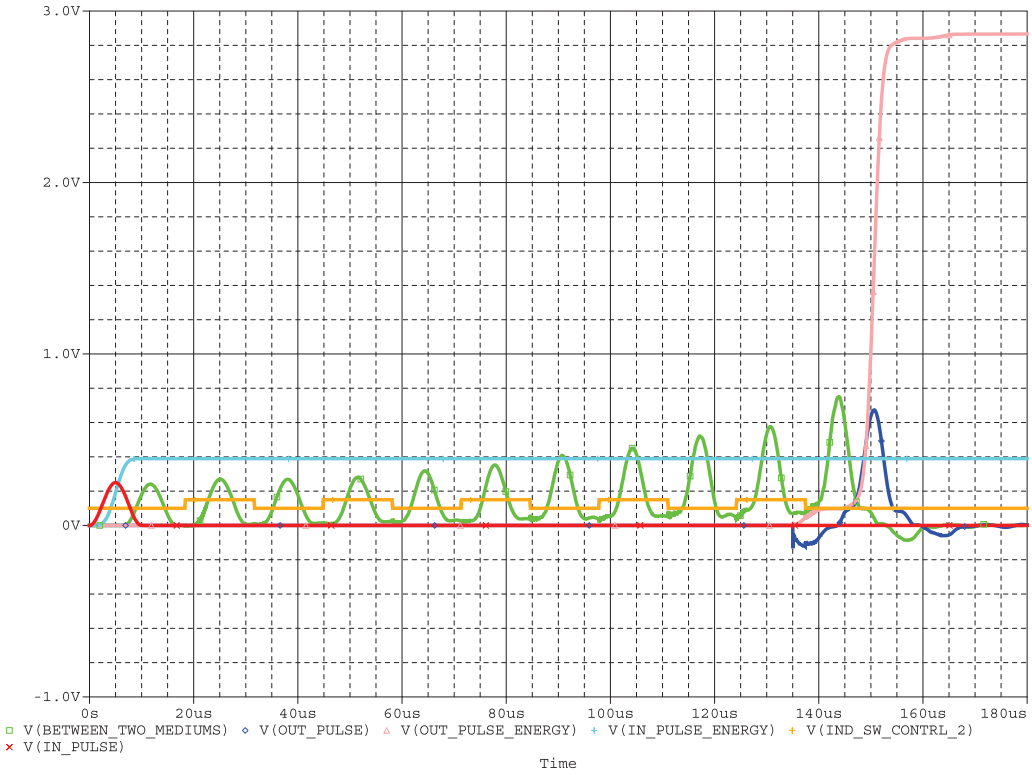

Figure 10: Energy accumulation in a transmission line with real elements

Initial Pulse Amplitude (V)	Initial Pulse Energy (nJ)	Energy Supplied by Switching Voltage Sources (nJ)	Total Energy Input into the System (nJ)	Output Pulse Energy (nJ)	Power Gain of the Initial Pulse (times)	Overall Power Efficiency of the System
0.25	0.39	4.95	5.34	2.87	7.4	54%
0.5	1.56	22.4	23.96	14.4	9.2	60%
0.75	3.5	53	56.5	34.4	9.8	61%
1	6.25	93.6	99.85	60.2	9.6	60%

Table 1

$\frac{1.26}{1.5} = 84\%$. To find true energy efficiency we have to know how much of the energy was supplied to the media to facilitate the temporal switchings.

Since inductors do not contribute to energy gain in our simulations (they are simply switched in and out when their currents are close to zero), the only source of the gain are the varactors, and, more specifically, voltage sources that control the values of the varactors. So, to calculate the energy from these sources, we calculate instantaneous values of $P = V * I$, integrate them over time, and then add the results from all sources together. This can be seen on the overall schematics in Fig. 8, at node VC SW Energy.

True energy efficiency of the system is calculated by taking the energy of the output pulse, as it is seen on the load resistor, and dividing it by the sum of energies of the input pulse and from voltage sources. The results are shown in Table 1. It can be seen that this efficiency can be as high as 61%, which is rather impressive. The Table 1 also shows that there is a limit on the voltages in the pulse - increasing the initial pulse amplitude eventually leads to deterioration of the performance due to the fact that we deal with "real" components: varactors start exhibiting their "diode-like" behavior with larger pulse voltages, for example.

To summarize the Stage 2 simulations:

1. A solution has been presented that allows the use of standard off-the-shelf components in LC-cells, and still maintain a requirement to preserve the characteristic impedance of the media.

2. It is possible to demonstrate the principle of energy accumulation with a reasonable number of "real" LC-cells without the active inductor equivalents or custom-made components.

3. The results of the simulations show impressive overall energy efficiency as high as 61%.

As a side note, this process of energy accumulation is akin to a class of amplifiers known as parametric amplifiers. As the name implies, these amplifiers work on the principle of changing a parameter in the system, rather than the use of active components (e.g. transistors). Varactors are one example of devices used in such amplifiers (the parameter being the capacitance of the varactor). And just like in our system, parametric amplifiers rely on specific timing as it relates to the signal being amplified. One of the main reasons for use of these amplifiers is the fact that the path of the amplified signal does not contain any active components and resistors required for proper operation, both of which generate various kinds of noise. As a result, parametric amplifiers are known to be very low-noise compared to "regular" amplifiers, albeit their use is limited to a few, very specific, areas.

Addendum

1. Although there is no specific "phase velocity" value in a lumped-element implementation, we can still assess it by assuming a typical LC-cell size (including all components and interconnects). With the real components used in this simulation, it is reasonable to assume that a cell will occupy a square with a side of approximately 20 mm. Given the values of L and C, we can say that our "media" have the following "phase velocities":

$$a_{slow} = \frac{1}{\sqrt{\frac{147\mu H}{0.02m} * \frac{360pF}{0.02m}}} \approx 0.87 * 10^5 m/s;$$

$$a_{fast} = \frac{1}{\sqrt{\frac{100\mu H}{0.02m} * \frac{240pF}{0.02m}}} \approx 1.29 * 10^5 m/s.$$

   As a point of reference, an optical would have been required to have its index of refraction of the order $3 * 10^8 * 10^{-5} \approx 3000$ to achieve similar phase velocity.

2. Temporal switches occur every $\approx 13.2\mu s$, which corresponds to a switching frequency of $\approx 76kHz$. This is dictated by the particular values of L and C, as well as the number of the LC-cells in the media.

3. This system was designed with a specific goal: to develop an approach that can be physically implemented with reasonable size and cost. As such, it has inherent limitations as compared to a "limitless and ideal" simulation. One of these limitations has to do with the shape and, more importantly, width of the initial pulse. It is unadvisable to try it with the width of the initial pulse that does not "fit" entirely within one of the two media due to the following:
   a) As it was mentioned earlier, it is important that currents through all inductors in both media are near zero when a temporal switching is occurring (to satisfy magnetic flux preservation). If the pulse is present in both media at these moments, this condition may not be satisfied everywhere. In addition, if there are currents flowing through inductors during the switchings, large voltage spikes will occur (the "flyback" effect, according to the formula: $V(t) = L * \frac{dI}{dt}$), which will have to be controlled to avoid damage to components.
   b) Due to the limited nature of the system (having only two media "re-used" over and over again), it will be almost impossible to interpret the results with wider pulses when different parts of the pulse energy overlap in space-time.
   These additional simulations show that, despite being restricted in nature due to design goals, this system is robust and shows consistent performance with respect to varying amplitudes of the initial pulse, as well as to the number of space-time switches.

References Cited

[1] Blekhman, I. I., and Lurie, K.A, "On Dynamic Materials". *Proc. Russian Acad. Sci. (Doklady)*, 37, 182–185, 2000.

[2] Lurie, K. A., *An Introduction to the Mathematical Theory of Dynamic Materials*. Vol. 15. New York: Springer, 2007, (Second Edition: 2017).

[3] Krylov, S., Gerson, Y., Nachmias, T. and Keren, U., "Excitation of Large Amplitude Parametric Resonance by the Mechanical Stiffness Modulation of a Microstructure". *J. Micromech. Microeng.*, 20(1):015041, 2010.

[4] Krylov, S., Ilic, B.R., Schreiber, D., Seretensky, S., and Craighead, H., "Pull-in behavior of Electrostatically Actuated Bistable Microstructures". *J. Micromech. Microeng.*, 18(5):055026, 2008.

[5] Krylov, S., Lurie, K.A., "Compliant Structures with Time-Varying Moment of Inertia and Non-zero Average Momentum and their Applications in Angular Rate Microsensors". *J. Sound. Vib.*, 330(20), 4875–4895, 2011.

[6] Oohira, F., Iwase, M., Matsui, T., Hosogi, M., Ishimaru, I., Hashiguchi, G., Mihara, Y., and Iino, A. "Self-hold and Precisely Controllable Optical Cross-connect Switches Using Ultrasonic Micro Motors". *IEEE J. Sel. Top. Quantum Electron.*, 10(3), 551-557,2004.

[7] Pelesko, J. A., and Bernstein, D. H., *Modeling of MEMS and NEMS*. CRC press, New York, N.Y.,2002.

[8] Rozenberg, Y. I., Rosenberg, Y., Krylov, V., Belitsky, G., Shacham-Diamand, Y., "Resin-bonded permanent Magnetic Films with Out-of-plane Magnetization for MEMS applications". *J. Magn. Magn. Mater.*, 305(2), 357-360, 2006.

[9] Lurie, K. A., Weekes, S. L., "Wave Propagation and Energy Exchange in a Spatio-Temporal Material Composite with Rectangular Microstructure". *J. Math. Anal. Appl.*, 314(1), 286–310, 2006.

[10] Lurie, K. A., Weekes, S. L., and Onofrei, D., "Mathematical Analysis of the Waves Propogation through a Rectangular Material Structure in Space-time", *J. Math. Anal. Appl.*, 355(1), 180-194, 2009.

[11] Morgenthaler, F.R., "Velocity Modulation of Electromagnetic Waves". *IRE Trans. Microw. Theory Tech.*,6(4):167-172, 1958.

[12] Xiao, Y., Maywar, D. N., and Agrawal, G. P., "Reflection and transmission of Electromagnetic Waves at a temporal Boundary". *Opt. Lett.*, 39 (3), 574-577, 2014.

[13] Berezovski, M. and Berezovski, A., "Numerical Simulation of Energy Localization in Dynamic Materials.", *Advances in Mechanics of Microstructured Media and Structures*. Springer, Cham, 75–83, 2018.